Effect of Cooling Rate and Alloying on the Transformation of Austenite

B. L. BRAMFITT AND A. R. MARDER

The pearlitic hardenability of a high-purity Fe-0.8 pct C alloy and zone-refined iron binary alloys containing Mn, Ni, Si, Mo, or Co was studied by means of hot-stage microscopy. The binary alloys were carburized in a gradient furnace to produce eutectoid compositions, thus eliminating proeutectoid phases. A special technique based on hot-stage microscopy was used to study the effect of cooling rate (10°F/min to 25,000°F/min) on the transformation of austenite and provided data for the construction of continuous cooling-transformation diagrams. From these diagrams critical cooling rates were obtained for hardenability calculations. It was found that molybdenum is the most effective element, followed by Si, Ni, Co, and Mn, in suppressing the pearlite transformation, *i.e.*, in increasing the hardenability of the alloys studied. The alloying additions were grouped into two classes according to their effect on hardenability: α-stabilizers (Mo and Si) and γ-stabilizers (Ni, Co, Mn), with the α-stabilizers being the more effective in improving hardenability.

LONG aware of the commercial importance of hardenability, metallurgists have over the years been studying the compositional and microstructural factors affecting hardenability in order to develop alloy design criteria, particularly for modern high-strength applications. For example, partly because of the stimulus of the property requirements for new steels for ships, aircraft, and ordnance in the early 1940's, Grossman,[1] followed by others,[2-4] developed some of the basic quantitative data for such alloy design needs. Their work allowed metallurgists to approximate the "ideal critical diameter" of a steel bar by using multiplying factors for chemical composition and grain size. Many steels were subsequently designed using this basic data for hardenability calculations, data which is still in wide use today.

Fundamental to the problems of designing alloys for optimum hardenability for specific applications is a sound knowledge of the mechanisms of alloying behavior and the complex role of multiple combinations of alloying elements in these mechanisms. In contradistinction to Grossman,[1] who postulates multiplicative alloy effects on hardenability, *per se*, Hollomon and Jaffe considered the effect of alloying on "pearlitic and bainitic hardenability," *i.e.*, the ability to avoid the pearlite.

Another source of information in this area was provided by the isothermal-transformation (I-T) diagrams resulting from a series of isothermal heat treatment studies.[5] These diagrams are useful in predicting the microstructural changes during isothermal transformation. Other investigations[6-8] resulted in a series of continuous cooling-transformation (C-T) diagrams that provide guidance to the alloy designer by predicting the phases that result upon continuous cooling conditions, *e.g.*, oil quenching.

B. L. BRAMFITT and A. R. MARDER are Engineer and Supervisor, respectively, Transformations and Strengthening Mechanisms Group, Alloy Development Section, Research Department, Bethlehem Steel Corporation, Bethlehem, Pa. 18016. This paper is based on a presentation made at a symposium on "Hardenability" held at the Cleveland Meeting of The Metallurgical Society of AIME, October 17, 1972, under the sponsorship of the IMD Heat Treatment Committee.

In the present work we studied the effect of continuous cooling on the transformation of binary iron-carbon as well as a number of high purity ternary alloys. The data thus obtained were then used to classify the kinetic behavior of alloying elements as γ-formers or α-formers.

Two techniques were developed for this study: a) a gradient furnace technique for producing alloys of eutectoid composition, and b) a procedure using the hot-stage microscope, by which we studied and recorded the thermal events and associated microstructural changes in alloys during cooling and transformation. Throughout the study, cinephotomicrography was used to accurately record the microstructural changes. For the present study only the extent of pearlitic transformation as a measure of hardenability has been considered. The hot-stage technique offered a fast method of studying individual alloying effects on this transformation product, thus yielding significant information on hardenability.

EXPERIMENTAL PROCEDURE

The starting materials for the hardenability studies were zone-refined iron binary alloys containing Mo, Ni, Co, Mn, and Si (Table I). Rods of these alloys, $\frac{1}{4}$ in. in diam, were cold-rolled into 20-mil sheet for further processing.

To produce high-purity binary and ternary eutectoid alloys we used a special gradient furnace technique[9] consisting of the dynamic carburization of the sheet material in a gaseous mixture of methane and hydrogen (1:20 ratio) at a temperature of 1800°F. Each specimen during carburization was passed through a steep temperature gradient of 3500°F/in. at a rate of 2.8×10^{-5} in./s, and the specimen obtained was entirely pearlitic, *i.e.*, free from proeutectoid phases. The carbon contents of the ternary alloys after carburization were higher (about 1 pct C) than those Bain and Paxton reported for the ternary eutectoids where the addition of a third alloying element lowers the carbon level to below 0.8 pct C.[10] The carbon content for the Fe-C binary alloy was consistent with the Fe-C phase dia-

Table I. Chemical Analysis of Alloys

	C	Mn	Si	Ni	Co	Mo
Binary Alloy	0.80	<0.01	<0.01	0.02		<0.002
low-nickel alloy	1.05*	T	T	0.46	ND	T
high-nickel alloy	0.94*	T	T	3.35	ND	T
low-cobalt alloy	0.94*	ND	ND	0.01	0.49	T
high-cobalt alloy	1.30*	ND	T	0.02	1.00	T
low-manganese alloy	1.00*	0.43	ND	T	ND	T
high-manganese alloy	1.00*	0.78	ND	T	ND	T
low-molybdenum alloy	1.00*	ND	ND	ND	ND	0.23
high-molybdenum alloy	1.06*	ND	0.005	0.001	ND	0.45
low-silicon alloy	1.00*	ND	0.30	T	ND	T

*Carbon analysis obtained after carburization in gradient furnace.
T–Trace, ND–None Detected

gram. We therefore tested the carburized specimens by reaustenitizing them in a standard furnace and allowing them to furnace-cool to find out whether the gradient treatment produced an equilibrium pearlitic structure under nongradient conditions; in no case were proeutectoid phases present in the binary or ternary alloys under investigation.

Producing an equilibrium eutectoid composition by means of the gradient technique is based on saturation of the austenite with carbon. At the austenitization temperature of 1800°F, the amount of carbon required for complete saturation in the binary Fe-C alloy system was about 1.5 pct. As each specimen passed through the steep temperature gradient, it ranged in temperature from 1800°F at one end to room temperature at the other end and the carbon concentration of the austenite decreased from the saturated amount down to that of the eutectoid concentration at the eutectoid temperature. As a matter of fact, in the iron-carbon binary phase diagram this concentration of carbon in the austenite follows a path along the A_{cm} line. Consequently, by the time the eutectoid temperature has been reached, the austenite of eutectoid composition has transformed completely to pearlite. Of course, in ternary systems the situation is more complicated; however, Yue,[11] using a technique similar to our gradient furnace technique, *i.e.*, zone-refining, has established accurate eutectic compositions for complex alloy systems consisting of four and six different elements.

The main advantage of our gradient furnace technique is that a eutectoid structure is easily obtained, whereas it may take several alloys and detailed chemical and metallographic analysis to obtain the same structure using melting and casting techniques, where the additional factor of segregation occurs during solidification. Carbon segregation exists in the gradient furnace specimen but only in the final portion of the specimen that transforms last. This high-carbon region can easily be removed and discarded.

The carburized specimens were cut into $\frac{1}{8}$-in. squares for the hot-stage microscope, a description of which has been published.[12] The hot-stage microscope was modified for this investigation to include a capability for the thermal analysis of phase transformations. With this modification, the hot-stage microscope becomes an excellent tool for the study of transformations. While a given transformation is being observed, microstructural changes can be photographically recorded at the same time as one records thermal history data such as thermal arrests, cooling rates and heating rates. A platinum/platinum-10 pct rhodium thermocouple was spot-welded to each specimen using the specimen as the hot junction, a thermocouple bead being undesirable because of the inhomogeneous temperature gradients during cooling rate studies. All heating and cooling treatments were performed under a high-purity argon atmosphere.

The specimens were placed in the furnace and heated to 1850°F for 2 min and then cooled at a controlled rate to room temperature. Cooling rates ranging from 10°F/min to 25,000°F/min were used for the experiments. The fast cooling rates were obtained by quenching the specimen with helium gas cooled to a temperature of −125°F. The slower cooling rates were obtained by controlling the furnace current by means of a motorized variable rheostat. All heat-treating cycles were recorded on a calibrated strip-chart recorder, and the actual cooling rate and thermal arrest temperatures were taken from the cooling curve.

During the cooling process the growth of pearlite and/or martensite was observed in the microscope using phase-contrast objectives. The growth of pearlite from austenite was barely discernible when compared with the formation of martensite, which is easily observed due to the surface upheaval created upon cooling. After each thermal cycle, the specimen was removed from the hot-stage and examined metallographically to make certain that the microstructure was consistent throughout the specimen and not merely a surface phenomenon.

The growth rate of the transforming phase can be accurately measured from the cinephotomicrographs. The technique allows one to measure the growth rate in any direction from the nucleation site as well as the growth rate of simultaneous events in the specimen. Accurate measurements can also be made during the impingement of two or more transformation products.

RESULTS AND DISCUSSIONS

Our results are discussed under three main headings: 1) results of our hot-stage microscopic study of the transformation of austenite, 2) the effect of cooling rate on the Fe-C binary alloy, and 3) the effect of cooling rate on Fe-C ternary alloys.

Hot-Stage Microscopy of the Transformation of Austenite

The visual results of any hot-stage technique depend on surface relief of the transformation product which produces a contrast effect that can be observed during transformation. There have been several previous hot-stage light microscopy studies to observe the formation of martensite[13] and bainite.[14-16] These two transformations involve a considerable amount of surface upheaval due to a shear mechanism. The formation of pearlite, however, has received little attention in the literature, probably because it is not easily detected by light optics. However, when phase-contrast objectives are used, the growth of pearlite from austenite can be seen in the hot-stage microscope. For example, Fig. 1 shows the sequence of growth of a pearlite nodule (arrow) at the juncture of three neighboring austenite

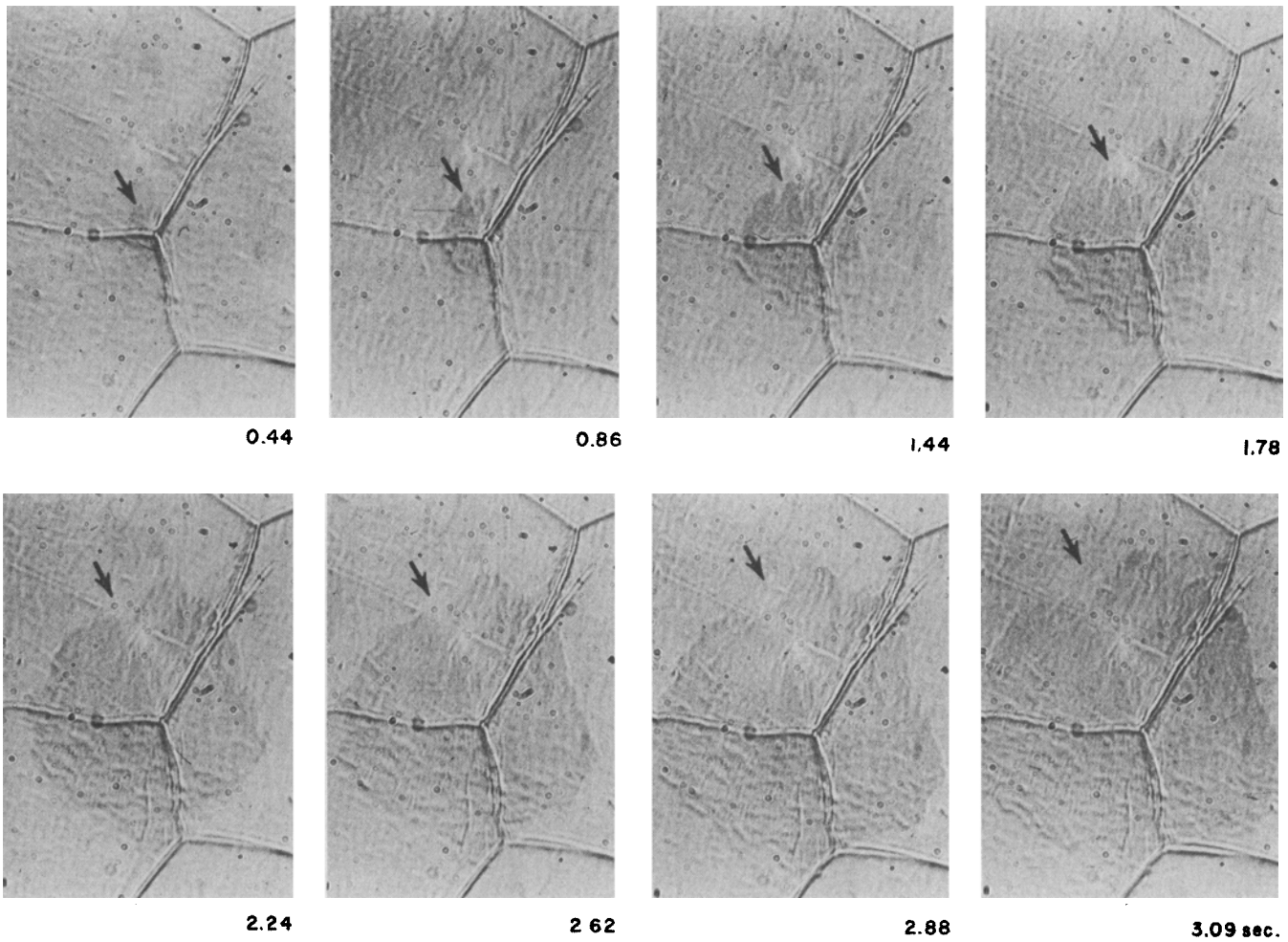

Fig. 1—Cinephotomicrographic sequence of growth of a pearlite nodule (arrow) at the junction of three austenite grains; cooling rate 4800°F and transformation temperature 1090°F. Magnification about 250 times.

grains. The cooling rate in this particular example was 4800°F/min, with the transformation taking place at 1090°F. If the growth process were interrupted by a fast quench with cold helium gas, the untransformed austenite would transform to martensite at the M_S temperature. An example of this technique is shown in Fig. 2. The actual surface relief (Fig. 2(*a*)) is shown along with the etched pearlite region (Fig. 2(*b*)). The pearlite nodules consist of many pearlite colonies of differing orientation, and the nodules generally nucleate at austenite grain boundaries and grow in a spherical geometry until they impinge on other nodules. In this case, the formation of plate martensite prevented impingement.

Throughout the investigation, specimens were polished and etched in cross section to make certain that the phenomenon observed on the surface had also taken place in the interior of the specimen. Fig. 3 shows a typical cross-section view at magnification 200 and 500 times of two different specimens that were rapidly quenched at a stage in the transformation to pearlite when nodule growth was occurring. As can be seen, the nodules nucleate and grow throughout the specimen thickness. It is important to note, however, that the spherical growth at the specimen surface seen in the microscope is not necessarily taking place at the nodule equator. In other words, the surface growth may represent only a portion of the nodule, the center of which is submerged below the surface plane. It is important to keep this in mind when considering growth-rate measurements on the surface. When, however, the nodule is sectioned, its center can be located and corrections in growth can be made using simple geometric relationships.

Although somewhat outside the scope of the present study, an example of the measurement of growth rate is given. A cinephotomicrographic series of the stages of growth of a pearlite nodule is shown in Fig. 4(*a*), which represents a cooling rate of 5300°F/min and a transformation temperature of 1090°F. The growth rate of 56 μm/s shown in Fig. 4(*b*) was measured from the nodule shown in Fig. 4(*a*) (arrow). The growth rate for the other nodule growing at the juncture of the three austenite grains is somewhat lower at 49 μm/s. These growth rates are in good agreement with the data of Frye *et al.*,[17] who reported an experimental value of 52.5 μm/s for a high-purity 0.78 pct C steel at a transformation temperature of 1094°F, and with the data of Hull *et al.*,[18] who reported a measured value of 65 μm/s for a high-purity 0.93 pct C steel at 1110°F. Their growth rates were obtained by means of the tedious salt-bath method, in which the specimens are allowed to isothermally transform for various periods of time and are then quenched to room temperature. The microstructures are then examined for the largest diameter nodule. The advantage of the hot-stage technique is that the measurements can be made on a single spec-

A

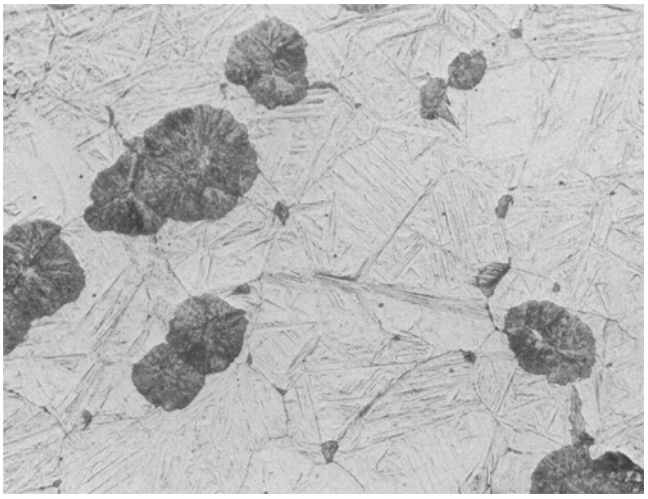

B

Fig. 2—Partially transformed and quenched specimen showing: (*a*) surface relief of specimen in hot-stage (unetched), and (*b*) polished and etched (picral) region below surface. Magnification 190 times.

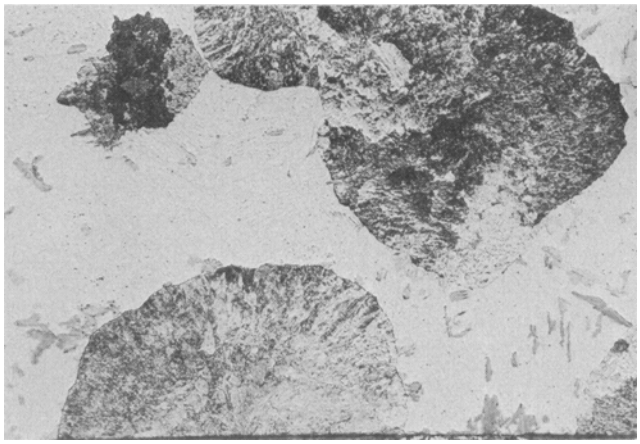

Surface 370X

Surface

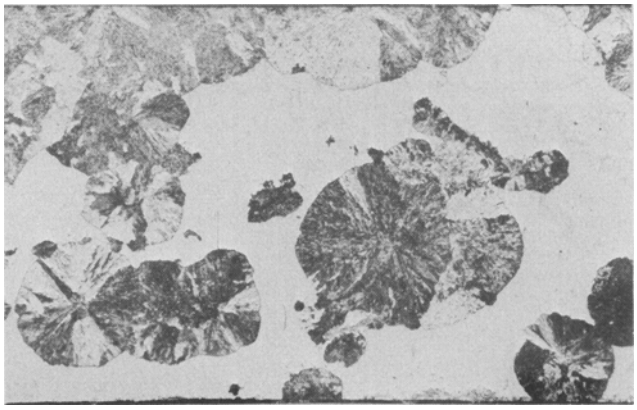

Surface 150X

Fig. 3—Cross-section views of the microstructure of pearlite nodules in partially transformed hot-stage specimens, showing nodule forming both at specimen surface and interior. Picral.

imen in which the growth rates of various nodules can be measured simultaneously. An interesting aspect of the growth rate curve in Fig. 4(*b*) is that this rate, which apparently fluctuates with time, does not change on impingement. Assuming that a "soft impingement" should take place, Cahn and Hagel[19] had theorized that the rate would decrease at this point.

The Effect of Cooling Rate on the Fe-C Binary Alloy

Specimens of the high-purity, iron-carbon binary alloy were subjected to cooling rates ranging from 12 to 25,000°F/min. The effect of cooling rate on the pearlite transformation temperature is shown in Fig. 5. A limiting cooling rate, *i.e.*, the critical cooling rate for this alloy, was reached at 25,000°F/min, at which point a mixture of both martensite and pearlite formed. The critical cooling rate for this study is defined as the cooling rate at which a substantial amount of martensite becomes observable in the light microscope. The suppression of the transformation temperature is generally expressed in terms of the "undercooling," ΔT, which is simply the difference between the equilibrium and actual transformation temperature. The undercooling increases with increasing cooling rate until the critical cooling rate is reached.

A comparison of our continuous cooling data with the isothermal data of Brown and Ridley[20] on an alloy of almost identical composition is shown in Fig. 6. As can be seen from Fig. 6, increasing the cooling rate significantly depresses the pearlite transformation start. Although this effect is also seen in the case of Brown and Ridley's data, the difference is even more magnified in their case by the elapsed time necessary for transfer of specimens to an isothermal bath. Although they do not discuss their transfer time from the austenitizing temperature to the isothermal bath, we encountered transfer times of up to two seconds in some of our own isothermal studies; thus, if transfer time were taken into account, their isothermal transformation start curve for pearlite would be moved to the right. Hence, on the basis of both types of data represented in Fig. 6, continuous cooling significantly lowers the pearlite start temperatures and moves the transformation to longer time, thus increasing hardenability. An example of the pearlitic structures found at various cooling rates is shown in Fig. 7. The letters

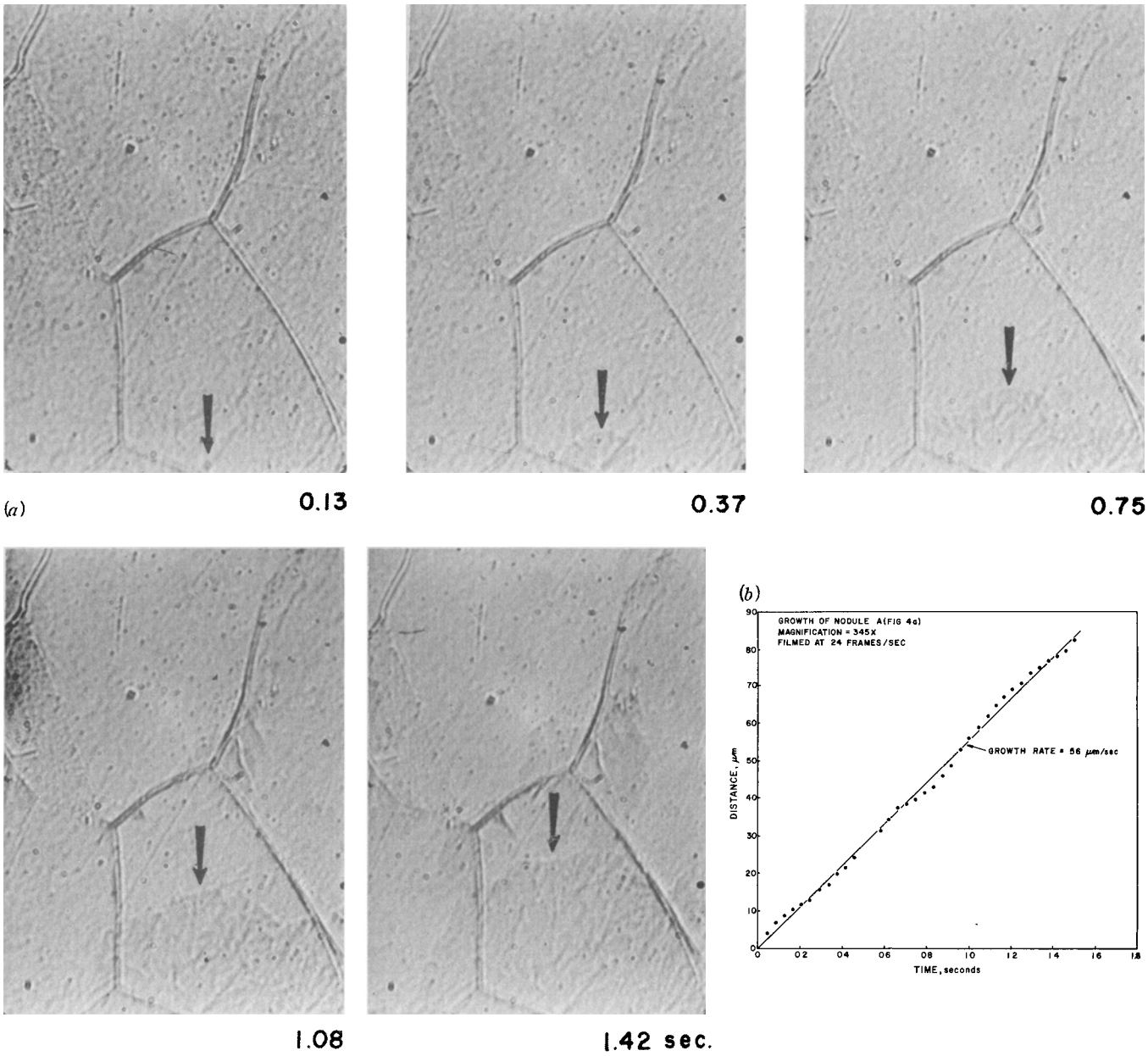

Fig. 4—(*a*) Cinephotomicrographic sequence of a growing pearlite nodule (arrow), cooling rate 5300°F per min and transformation temperature 1090°F. (*b*) The growth rate curve for the nodule in (*a*). Magnification about 350 times.

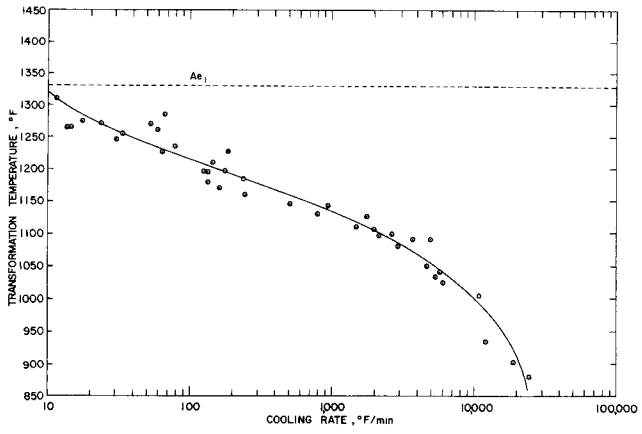

Fig. 5—The effect of cooling rate on the pearlite transformation temperature for the iron-0.8 pct carbon alloy.

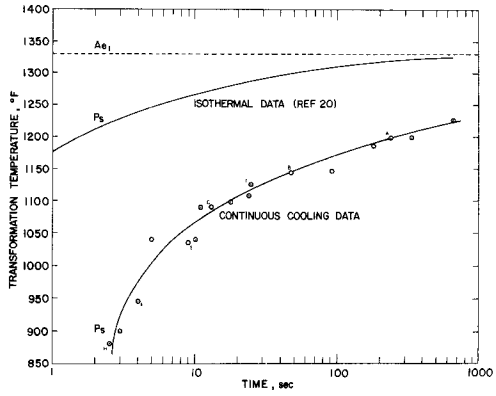

Fig. 6—A comparison of continuous cooling transformation data for the Fe-0.8 pct C alloy with the isothermal transformation data of Brown and Ridley for a similar alloy.

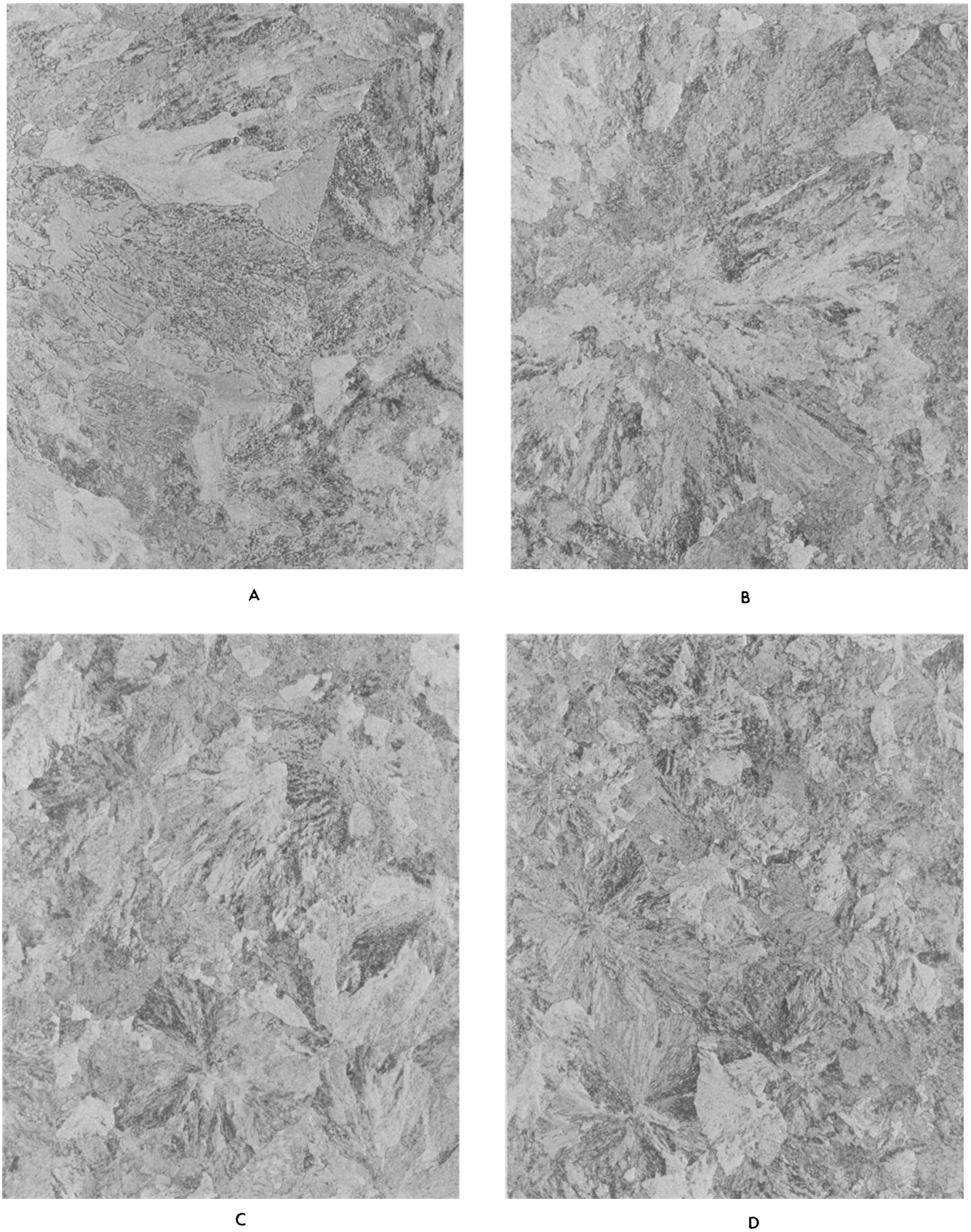

Fig. 7—A series of photomicrographs representing the structures produced at eight different cooling rates for the Fe-0.8 pct alloy. The letters correspond to the lettered data points in Fig. 6. Picral. Magnification 200 times.

correspond to the lettered data points in Fig. 6. It is seen that as the cooling rate increases or time for transformation decreases, the pearlite structure represented by the nodules becomes smaller. At *G* and *H* martensite forms and surrounds the already growing pearlite nodules.

The development and growth of nodules in the critical cooling range can be seen in Fig. 8, where several

E

F

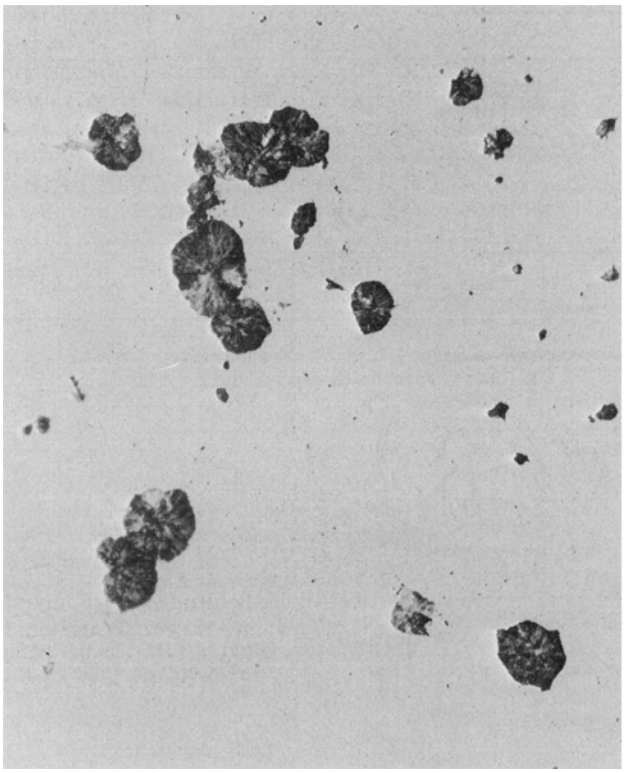

G

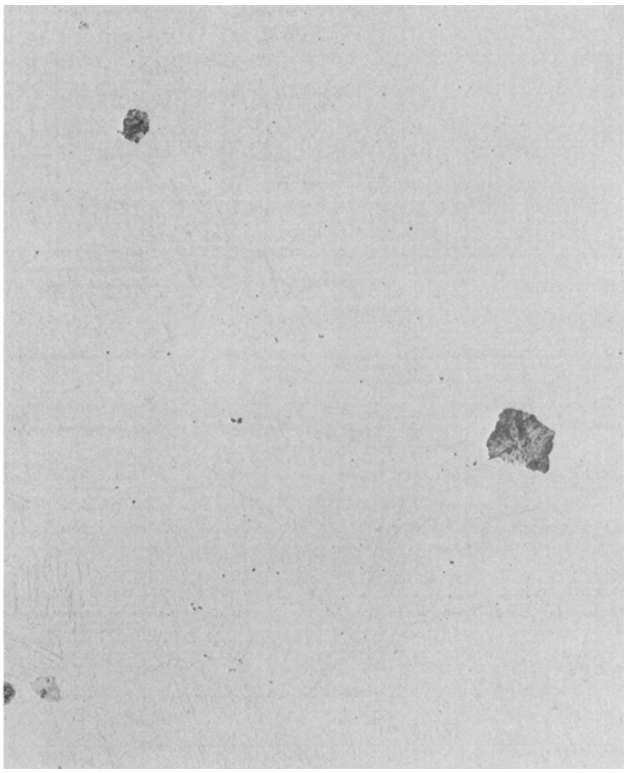

H

Fig. 7—Continued

small pearlite nodules grew to the limiting size dictated by the residence time at the nose of the C-T diagram. This example has a cooling rate between the cooling rates of G and H in Fig. 6. The cinephotomicrographs in Fig. 8 represent the limit of growth of the pearlite nodules (arrows) at 0.91 s, the start of martensite formation at 3.51 s, continuing formation of martensite at 3.84 s, and finally the end of transformation at 5.71 s.

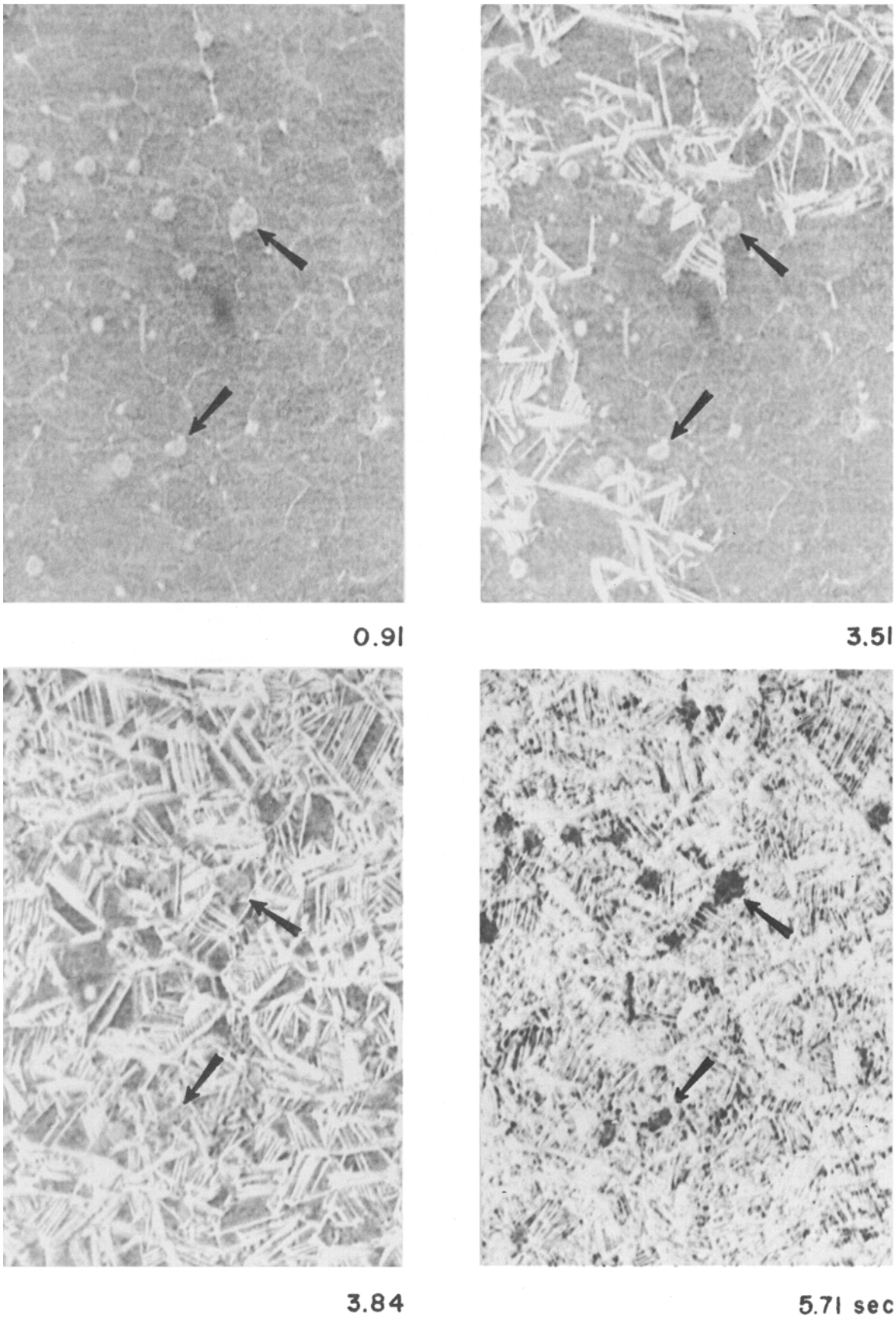

Fig. 8—Cinephotomicrographs representing the critical cooling rate for the Fe-0.8 pct C alloy (near data points *G* and *H* in Fig. 7). This series shows the limit of growth of the pearlite nodules (arrow) followed by the formation of martensite. Magnification about 440 times.

The delay time from the finish nodule growth to the beginning of martensitic growth was 2.60 s.

The Effect of Cooling Rate on Fe-C Ternary Alloys

The effect of cooling rate on the pearlite transformation temperatures of the five ternary alloys containing Ni, Mn, Co, Mo, or Si is shown in Figs. 9(*a*) through (*e*), respectively. Two composition levels are shown for each alloy, excepting the silicon one. The cooling rates varied from 71°F/min to the critical cooling rate, which is indicated in each graph. To compare the relative effects of alloy on the *C-T* diagram behavior, we included Fig. 10, which shows the composite *C-T* diagrams for a constant alloy level of 0.45 wt pct (except for Si at a level of 0.3 wt pct). In general, it can be seen that molybdenum has the greatest effect in suppressing the transformation temperature, silicon, nickel, cobalt, and manganese following in descending order. This trend is shown in Fig. 11, where the suppression of the transition temperature is expressed in terms of percent alloy at a constant cooling rate (10°F per min). The trend for molybdenum and silicon is different from that for nickel, cobalt, and manganese. This difference in the two trends is consistent for the entire range of cooling rates and indicates that molybdenum is the most effective alloying addition for improving hardenability. The dependency of critical cooling time and critical cooling rate on alloy content is shown in Figs. 12 and 13. Again, the behavior of molybdenum and silicon differs from that of the other elements, a result which is consistent with the findings above. The alloys appear to separate out according to whether they are substitutional austenite stabilizers, represented by Ni, Mn, Co, or ferrite stabilizers, *i.e.*, the γ-loop formers, Mo and Si. When the basis of comparison is critical cooling rate to form martensite per wt pct alloy (slope of the two straight lines in Fig. 13), it is seen that the γ-stabilizers have a slope of 6000°F per min per wt pct alloy whereas the α-stabilizers have a slope of 25,000°F per min per wt pct alloy. That is, it is easier to form martensite or increase hardenability with the α-stabilizers.

Our results were compared with the early hardenability data of Grossman[1] and Kramer *et al.*,[2] as well as with the later data of Kramer *et al.*[21] and Manning et al.[22] The multiplying factors from these investigations taken at 0.45 wt pct are listed in Table II. The trends shown by these results, particularly those of Manning *et al.*[22] are in agreement with our findings, except for silicon, which we found has a greater effect on hardenability based on its *C-T* diagram behavior.

The breakdown of the alloys into α-stabilizers and γ-stabilizers is in qualitative agreement with the concept of the two alloy classes first proposed by Zener.[24] He stated that one class retarded the formation of both pearlite and bainite, with manganese and nickel being among the most prominent in this class. Zener noted that the second class which includes molybdenum, retards the formation of only pearlite, a phenomenon which he believed is associated with the carbide-forming tendencies of this class.

The degree of potency of the α-stabilizers and γ-stabilizers is shown in Table III where hardenability is compared using a method proposed by Grossman,[1]

Table II. Comparison of Hardenability Data

	Multiplying Factor			
Element	Ref. 22, 1967	Ref 21, 1946	Ref. 1, 1942	Ref. 2, 1944
Mo	2.9	2.9	2.4	2.4
Mn	1.3	1.2	2.5	2.9
Si	1.2	1.3	1.4	1.5
Ni	1.1	1.4	1.2	1.1
Co	–	–	–	1.0

Table III. Hardenability Comparison of Alloying Additions

	Alloying Element	Wt Pct Alloy/Pct Increase M.F.	Ref.
	Ti	0.014 to 0.080	3, 25
	V	0 04 to 0.30	1, 3
	Mo	0.16 to 0.20	1, 3
α-stabilizers	Zn	0 20	3
	Cr	0.22 to 0.36	3, 22
	Al	0.55	3
	Si	0.55 to 0.75	1, 25
	Mn	0.60 to 0.80	21, 25
γ-stabilizers	Ni	1.15 to 1.30	1, 25
	Cu	>1.5	25

i.e., amount of alloy per 50 pct increase in the multiplying factor. As can be seen, the α-stabilizers require much less alloying addition than the γ-stabilizers for an equivalent increase in hardenability.

Although this proposal suggests that certain α-stabilizing elements, *i.e.*, Ti, V, Zr, Cr, W, and Nb, improve the hardenability of steel, the competing process of carbide precipitation in the austenite robs it of both carbon and alloy addition, thus lowering hardenability. Hardenability multiplying factor results show that vanadium[1] and titanium[25] have factors approaching 2 at 0.03 pct alloy additions which are greater than that of molybdenum, the most effective alloy. Unfortunately, beyond 0.03 pct, titanium or vanadium carbide precipitation occurs and the multiplying factor begins to drop.

SUMMARY

The effect of cooling rate (10°F per min to 25,000°F per min) on the transformation of austenite to pearlite and martensite in a eutectoid binary Fe-0.8 pct C alloy and ternary Fe-C eutectoid alloys with Mo, Mn, Ni, Co, and Si was studied by means of hot-stage cinephotomicrography. Continuous cooling transformation diagrams were constructed, and critical cooling rates, i.e., the cooling rates necessary to form martensite, were used to determine the effect of the alloys in improving hardenability. These determinations provided the basis for dividing the alloys into two groups:

1) The α-stabilizers, Mo and Si.
2) The γ-stabilizers, Mn, Ni, and Co.

The α-stabilizers showed the strongest effect in improving hardenability.

The hot-stage technique is ideally suited for hardenability studies since thermal, kinetic, and morphological data can be obtained simultaneously for the transformation of austenite into one or more of its transformation products.

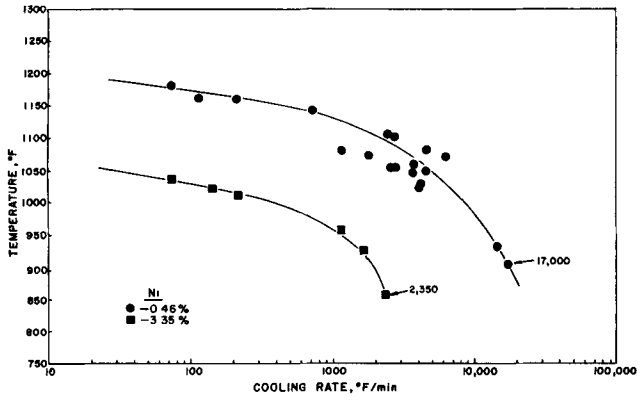

(a)

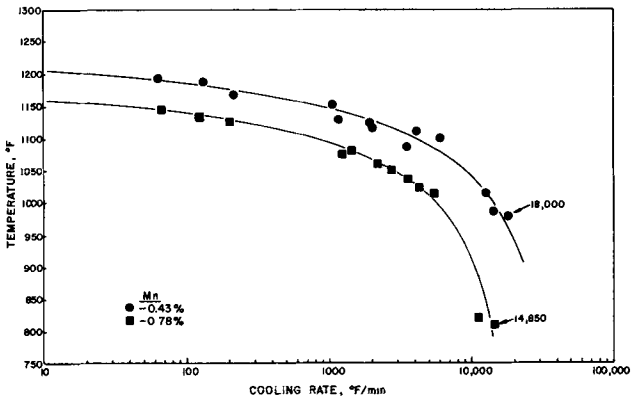

(b)

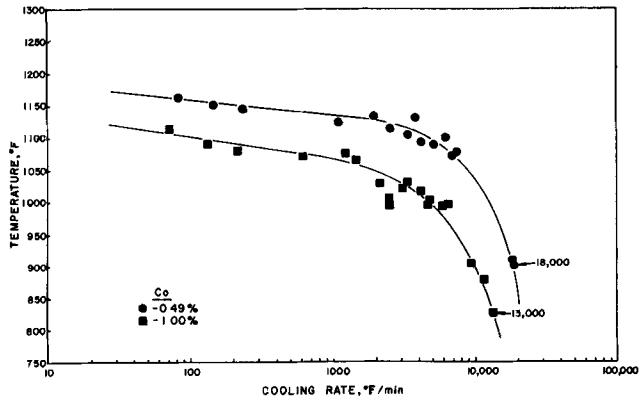

(c)

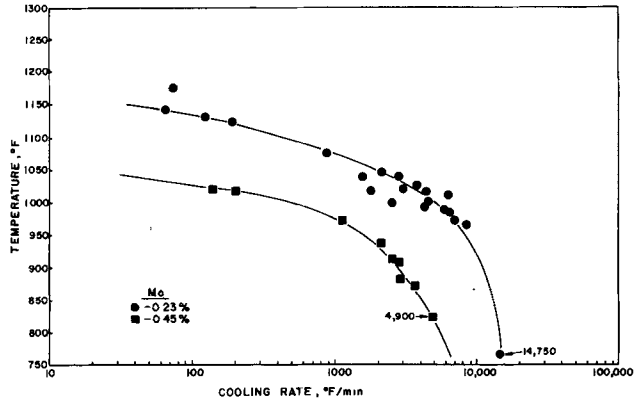

(d)

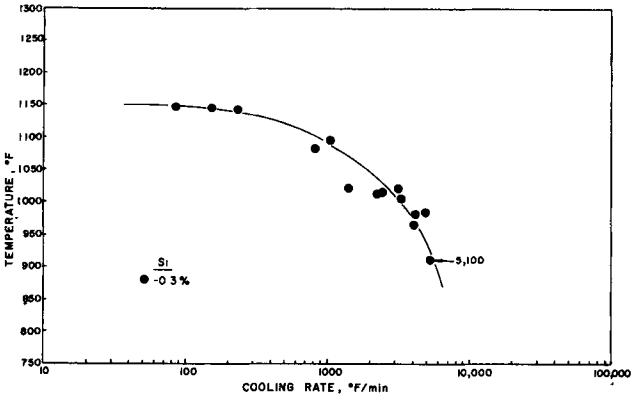

(e)

Fig. 9—The effect of cooling rate on the transformation temperature of ternary eutectoid Fe-C alloys containing: (*a*) 0.46 pct and 3.35 pct Ni, (*b*) 0.43 pct and 0.78 pct Mn, (*c*) 0.49 pct and 1.00 pct Co, (*d*) 0.23 pct and 0.45 pct Mo, and (*e*) 0.30 pct Si.

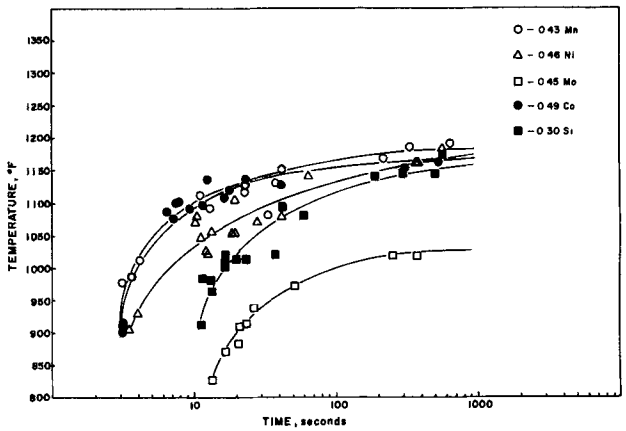

Fig. 10—Continuous cooling transformation diagrams for the ternary eutectoid alloys at a constant concentration of 0.45 wt pct, except for silicon, which was only a 0.3 wt pct addition.

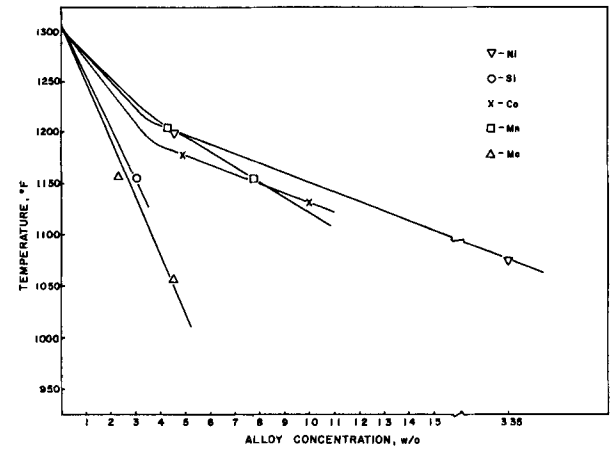

Fig. 11—The effect of alloy concentration on the transformation temperature at a constant cooling rate of 10°F per min.

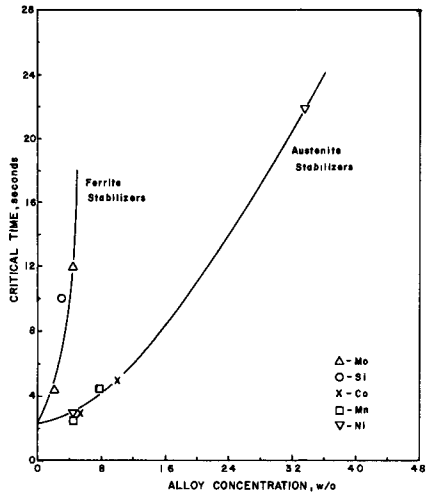

Fig. 12—Plot of the effect of alloy concentration vs critical time, demonstrating the contrasting behavior of ferrite and austenite stabilizers.

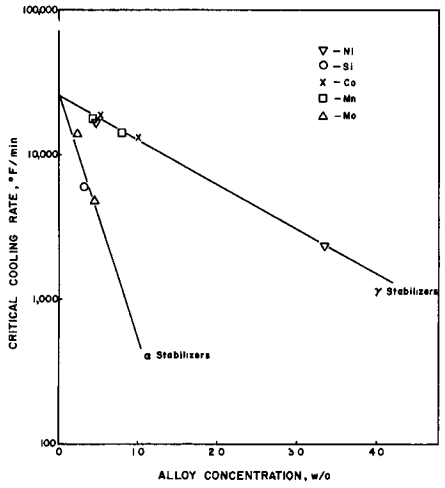

Fig. 13—Plot of the effect of alloy concentration vs critical cooling rate, demonstrating the contrasting behavior of ferrite and austenite stabilizers.

ACKNOWLEDGMENTS

The authors wish to express appreciation to J. R. Kilpatrick, A. O. Benscoter, R. E. Steigerwalt, J. C. Hlubik, W. A. Beveridge, and P. M. Giles. The authors also appreciate the assistance of B. S. Mikofsky for his input in the preparation of this manuscript.

REFERENCES

1. M. A. Grossmann *Trans. TMS-AIME,* 1942, vol 150, p. 227.
2. I. R. Kramer, R. H. Hafner, and S. L. Toleman *Trans. TMS-AIME,* 1944, vol 158, p 138.
3 W. Crafts and J. L. Lamont *Trans. TMS-AIME,* 1944, vol. 158, p. 157.
4 "Symposium on Hardenability," October 1945, *Trans. TMS-AIME,* 1946, vol. 167, p. 599.
5. *Isothermal Transformation Diagrams,* U. S. Steel, 1963.
6 C. A. Liedholm *Metal Progr.,* 1944, vol. 45, p. 95.
7. W. Steven and C. Mayer *JISI,* 1953, vol. 147, p. 33
8. D. J. Blickwede and R. C. Hess *Trans ASM,* 1957, vol. 49, p. 427.
9. B. L. Bramfitt and A. R. Marder *IMS Proc.,* 1968, p. 43.
10. E. G. Bain and H. W. Paxton. *Alloying Elements in Steel,* ASM, 1961, 2nd ed., p. 112.
11. A. S. Yue *Met. Trans.,* 1970, vol. 1, p 19
12. A. O. Benscoter, J. R. Kilpatrick, R. P. Wolf, and A. R. Marder. *Microstructures,* 1970, vol. 1, p. 25.
13 A. R. Marder and G. Krauss *Trans. ASM,* 1969, vol. 62, p. 957.
14. G. R. Speich and M. Cohen: *Trans. TMS-AIME,* 1960, vol. 218, p. 1050.
15. G. R. Speich: *Decomposition of Austenite by Diffusional Processes,* Interscience, 1962, p. 353.
16. R. H. Goodenon, S. J. Matas, and R. F. Hehemann· *Trans TMS-AIME,* 1963, vol. 227, p. 651.
17. J. H. Frye, E. E. Stansbury, and D. L. McElroy *Trans. TMS-AIME,* 1953, vol 197, p. 219.
18. F. C. Hull, R. A. Colton, and. R. F. Mehl: *Trans. TMS-AIME,* 1942, vol. 150, p 185.
19. J. W. Cahn and W. C. Hagel: *Acta Met.,* 1963, vol. 11, p. 561.
20. D. Brown and N. Ridley: *JISI,* 1969, vol 207, p. 1232.
21. I. R. Kramer, S. Siegel, and J. G. Brooks *Trans. TMS-AIME,* 1946, vol. 167, p. 670.
22. R. D Manning, H. M. Reichhold, and J. M. Hodge· *Symposium Transformation and Hardenability in Steels,* Climax Moly. Co., 1967, p. 169
23. J. H. Hollomon and L. D. Jaffe· *Trans. TMS-AIME,* 1946, vol. 167, p. 601.
24. C. Zener: *Trans. TMS-AIME,* 1946, vol. 167, p. 550.
25. G. F. Comstock: *Trans. TMS-AIME,* 1946, vol. 167, p. 719.